SCIENTIFIC REPORTS

OPEN

SUBJECT AREAS:
HETEROGENEOUS CATALYSIS
CARBON NANOTUBES AND FULLERENES
FUEL CELLS
ELECTROCATALYSIS

Received
28 March 2013

Accepted
27 June 2013

Published
23 July 2013

Correspondence and requests for materials should be addressed to R.C.H. (haddon@ucr.edu)

Functionalized Single-Walled Carbon Nanotube-Based Fuel Cell Benchmarked Against US DOE 2017 Technical Targets

Neetu Jha[1], Palanisamy Ramesh[2], Elena Bekyarova[1,2], Xiaojuan Tian[1], Feihu Wang[3], Mikhail E. Itkis[1,2] & Robert C. Haddon[1,3,4]

[1]Center for Nanoscale Science and Engineering, Departments of Chemistry and Chemical & Environmental Engineering, University of California – Riverside, Riverside, California 92521, USA, [2]Carbon Solutions Inc., 1200 Columbia Ave., Riverside, California 92507 USA, [3]Center for Nanoscale Science and Engineering, Department of Physics and Astronomy, University of California - Riverside, Riverside, California 92521, USA, [4]Department of Physics, King Abdulaziz University, Jeddah 21589, Saudi Arabia.

Chemically modified single-walled carbon nanotubes (SWNTs) with varying degrees of functionalization were utilized for the fabrication of SWNT thin film catalyst support layers (CSLs) in polymer electrolyte membrane fuel cells (PEMFCs), which were suitable for benchmarking against the US DOE 2017 targets. Use of the optimum level of SWNT -COOH functionality allowed the construction of a prototype SWNT-based PEMFC with total Pt loading of 0.06 mg_{Pt}/cm^2 - well below the value of 0.125 mg_{Pt}/cm^2 set as the US DOE 2017 technical target for total Pt group metals (PGM) loading. This prototype PEMFC also approaches the technical target for the total Pt content per kW of power (<0.125 g_{PGM}/kW) at cell potential 0.65 V: a value of 0.15 g_{Pt}/kW was achieved at 80°C/22 psig testing conditions, which was further reduced to 0.12 g_{Pt}/kW at 35 psig back pressure.

The polymer electrolyte membrane fuel cell (PEMFC) operating on hydrogen fuel has been identified as a clean energy source and is expected to reduce fossil fuel dependence[1–3]; a major hindrance to the commercialization of the PEMFC is the high cost associated with the Pt catalyst which continues to increase[2,3]. The US Department of Energy (DOE) has established 2017 technical target for reduction of the total Pt group metal (PGM) loading to 0.125 mg/cm^2, a significant decrease over the Pt loading of 0.4–1.0 mg/cm^2 used in current PEMFCs[4,5]. This can be translated to the Global target, which requires less than 10 g of platinum per car by the year 2020 compared to the 80 g of platinum in the current state-of-the-art commercial fuel cell cars[6]. Further decrease in the Pt loading requires the development of novel catalysts, which can improve the kinetics and thermodynamics of the oxygen reduction reaction (ORR) at the cathode[7–26]. In recent years a number of novel catalyst systems with reduced PGM content have been proposed including Pt alloys[10,12,16,18], core-shell Pt nanoparticles[11,19–21], Pt on whiskers and Pt nanotubes[3,22,23], and platinum-free catalytic systems[17,24–26]. The second direction, which is addressed in the present manuscript, relates to the improvement of the catalyst support layers (CSL) at the cathode and anode; the CSL governs the efficiency of catalyst utilization by maintaining the correct balance of reactants and products at the triple-phase interface[27–29].

The most commonly used catalyst support is carbon black (CB), but in the last decade a number of carbon-based nanostructured materials with high surface area and porous structures, such as SWNTs, multiwall carbon nanotubes (MWNTs), carbon nanofibers, nanohorns, and recently graphene, have received increasing attention[17,29–39]. Our recent efforts were devoted to the development of ultra-thin carbon nanotube CSLs with ultra-low Pt loading based on SWNTs, MWNTs[27,40,41], and SWNT-MWNT hybrid[28]; a related development was recently presented in a SWNT-carbon nanofiber hybrid structure[29].

In the present manuscript, we present a comprehensive study of the effect of chemical functionalization of SWNTs on the morphology and physical properties of the SWNT based CSL in relation to the electrochemical activity of the supported Pt catalyst. The degree of -COOH functionalization of the SWNTs was optimized, thereby allowing a reduction of the Pt loading to the level of 0.06 mg_{Pt}/cm^2 while the Pt content per kW of generated power at 0.65 V was reduced to 0.12 g/kW; both parameters benchmark favorably against the DOE 2017 technical targets. It should be noted that the DOE targets are set for an integrated 80 kW_{net} system which includes multiple MEA stacks and other auxiliary components. Nevertheless, the individual MEAs presented here constitute prototype cells which serve as precursors to the construction of complex integrated systems, so the

discussion of their performance in terms of DOE targets is appropriate, although the reliability requirements will be more rigorous in commercial systems. The SWNT thin film based CSL involves wet-ink processing that is easily scalable and fully compatible with conventional catalyst layer coating technologies.

Results

For optimization of the SWNT-based CSL, four different chemical processing routes (Figure 1), were applied to as-prepared electric arc synthesized SWNTs (AP-SWNTs)[42,43]. The first route included high temperature oxidation of AP-SWNTs in air for removal of amorphous carbon impurities followed by dissolution of the oxidized metal catalysts in dilute hydrochloric acid; this process resulted in purified non-functionalized SWNTs (SWNT-NF) with an undetectable concentration of COOH groups. Two other processing routes began with a 90 min, 16 M nitric acid reflux followed by low speed centrifugation[44], which is known to introduce carboxylic acid groups into the SWNTs, although acid-base titration experiments show that the concentration of phenol and lactone functionalities is negligible[45].

The solid obtained after decantation is subsequently referred to as purified, medium -COOH functionality SWNTs (SWNT-MF, 2 ± 0.4% COOH/carbon atom)[46–48]. Base treatment of the SWNT-MF material partially removes the carboxylated carbon fragments from the SWNTs[48], and results in purified, low COOH functionality SWNTs (SWNT-LF, 1 ± 0.2% COOH/carbon atom). The fourth route was comprised of 3 steps: 1) 3 hour, 16 M nitric acid treatment; 2) low speed centrifugation to remove amorphous carbon and oxidized catalyst; and 3) high speed centrifugation to remove graphitic nanoparticles[47]; the resulting product corresponds to purified, high functionality SWNTs (SWNT-HF, 4 ± 1% COOH/carbon atom).

As shown in the process flow diagram (Figure 1), the Pt nanoparticles were attached to the SWNT surface of all four SWNT products at targeted Pt loading of 30 wt% using the ethylene glycol based *in-situ* reduction process[49]. The actual Pt loading was evaluated by thermogravimetric analysis (TGA) taking into account the difference in TGA metal residue of SWNT materials before and after Pt deposition (Supplementary Information Figure S1). The resulting values of the Pt loading for all products were in the range 28–32 wt% with the Pt loading slightly increasing with the content of the carboxylic groups due to improved anchoring of Pt nanoparticles to the SWNT functionality (Supplementary Information Table S1). Inductively coupled plasma mass spectrometry (ICP), independently confirmed the validity of the TGA analysis for determination of Pt loading. The Pt-loaded SWNTs were dispersed in ethanol at a concentration of 0.1 mg/mL and deposited on a carbon fiber paper gas diffusion layer (GDL) coated with a hydrophobic microporous layer (SGL-GDL 25BC) by a vacuum filtration process in which the carbon fiber paper is used as the filtration membrane thereby leading to a GDL that is uniformly coated with the Pt-loaded SWNTs in the form of a thin film. The total amount of Pt-SWNT material in the dispersions was calculated to target an electrode loading of 0.03 mg_{Pt}/cm^2 (see Supplementary Information), approximately an order of magnitude less than that used in typical commercial PEMFCs.

SEM images of the thin films of Pt-loaded SWNTs are presented in Figures 2(a–d) and are strongly dependent on the degree of COOH content. The Pt-SWNT-NF film (Figure 2a) shows high porosity and large bundles, up to 100 nm in diameter, as a result of the strong van

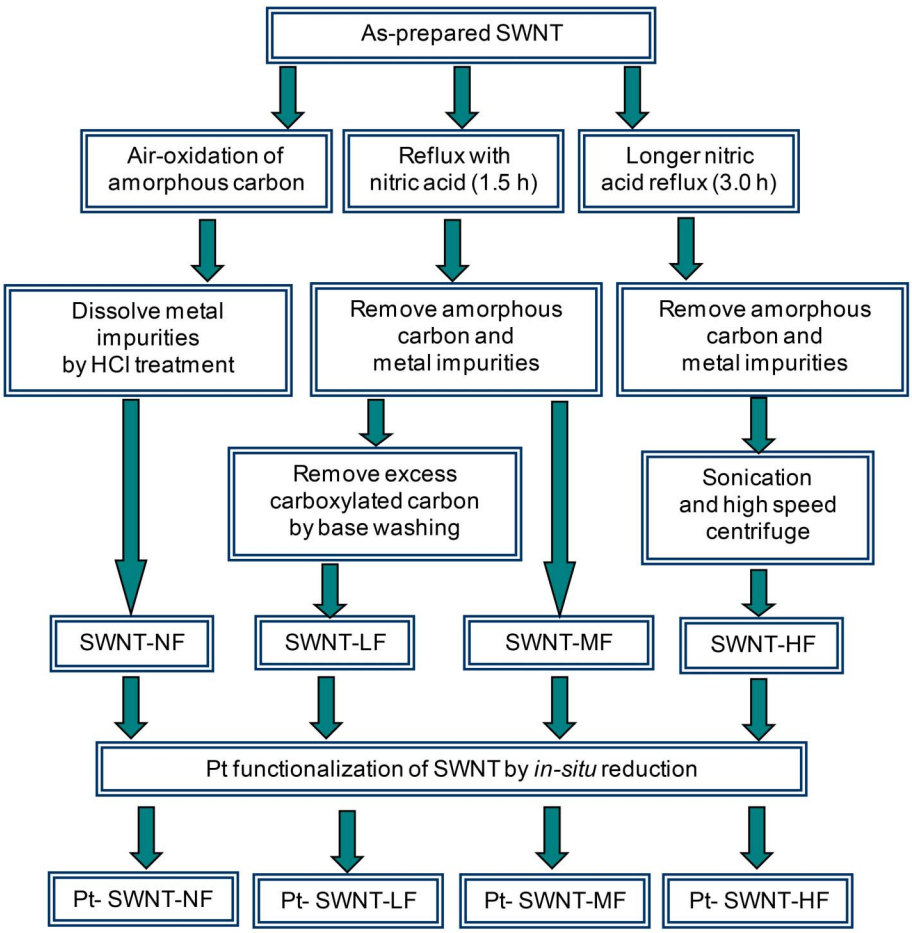

Figure 1 | Chemical processing routes for preparation of SWNT materials. The concentration of carboxylic acid groups is varied by the processing method.

der Waals attraction between the clean graphitic walls of the purified SWNTs which are free of surface functionalities. As the concentration of the surface functional groups increases the van der Waals interactions are inhibited and the average SWNT bundle size decreased in the following sequence: 15 nm (SWNT-LF), 7 nm (SWNT-MF), 4 nm (SWNT-HF) (SI, Table S1). With decreasing bundle size the pore size of SWNT film diminishes (Figure 2, a–d); at high COOH content (Pt-SWNT-HF, Figure 2d) the film consists of densely packed thin SWNT bundles with very small pore size.

TEM images showing the distribution of the Pt nanoparticles on the SWNT surfaces are presented in Figure 2e–2h; the imaging confirms the decreased bundle diameter as a result of the progressively increasing carboxylic acid content in the SWNT samples. The size of the individual Pt nanoparticles is between 1 and 5 nm (mean value of 2.2–2.4 nm) for all materials (Figure S2), but the degree of aggregation of the particles increases significantly with decreasing COOH content. For example, in the case of the SWNT-HF and SWNT-MF materials, the Pt nanoparticles are well separated and uniformly distributed on the surface of SWNT bundles, presumably as a result of platinum coordination by carboxylate groups, while in the case of the non-functionalized SWNT-NF material the Pt particles aggregate to form line-type fragments oriented along the SWNT bundles as a result of the high mobility of platinum on graphitic surfaces.

Figure 3 shows the degree of functionalization, apparent density, and Brunauer, Emmett and Teller (BET) surface area of the SWNT materials. As discussed earlier, the concentration of COOH groups increases from 0 to 4% per carbon atom between the extreme cases of non-functionalized and highly functionalized SWNTs as shown in Figure 3a. The apparent density of the SWNT films was calculated on the basis of their weight and geometrical dimensions and shows an increase (Figure 3b) in correlation with the decreased porosity and increased packing density of the SWNT network as the COOH content increases (Figure 2a–2d). The BET surface area shows a decrease of two orders of magnitude with increasing COOH content (Figure 3c); this can be related to blocking of the inter-bundle

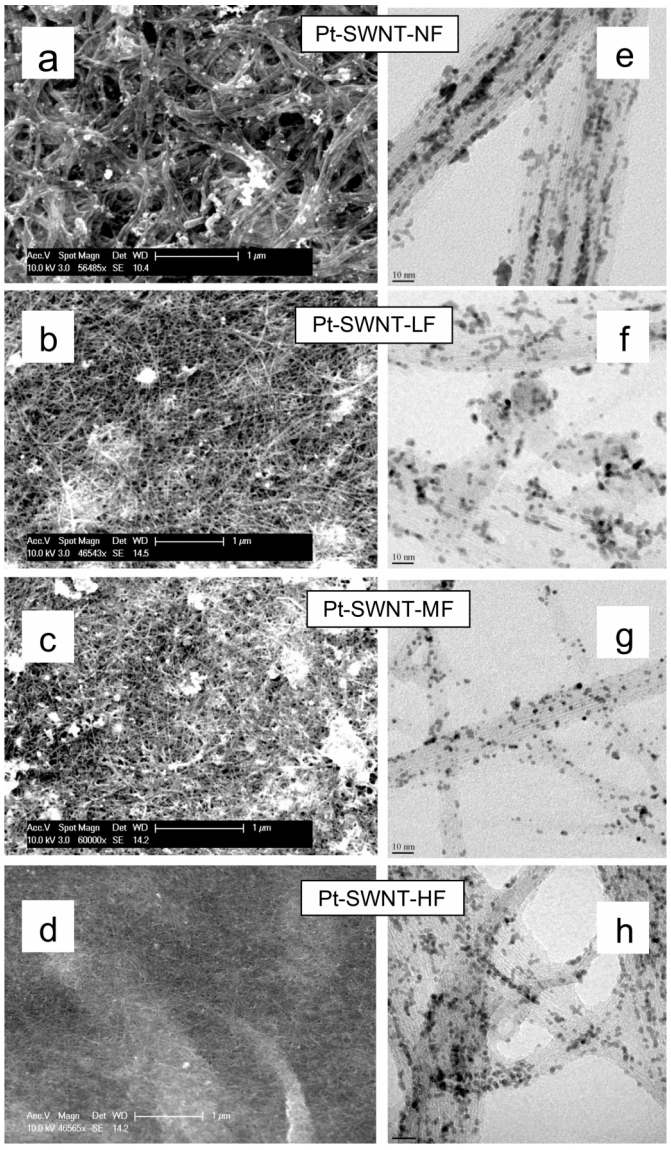

Figure 2 | SEM and TEM images of Pt supported SWNTs. (a–d) SEM images and (e–h) TEM images.

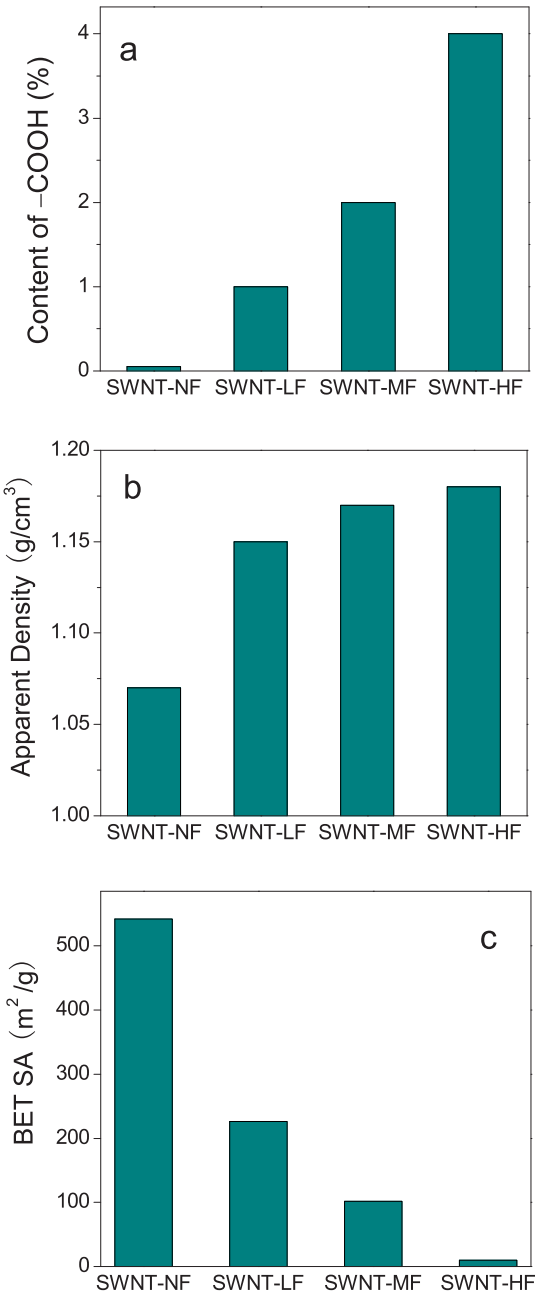

Figure 3 | Degree of functionalization, density and surface area of SWNT materials. (a) COOH functional group content, (b) Apparent density and (c) BET surface area of SWNT materials.

galleries and intra-bundle interstitial channels by the -COOH groups and carboxylated carbon fragments.

Figure 4 presents measurements of the electrochemical surface area (ECSA) of the CSL, an important characteristic which largely defines the fuel cell performance. Conventional measurements of ECSA involve the preparation of an ultrathin film of catalyst layer on a glassy carbon electrode designed to exclude diffusion problems[50], however, the same surface area is not always observed in an actual gas diffusion electrode configuration[30,51] for fuel cells utilizing 0.5–1.0 mg of Pt/cm^2 in a 15–30 μm thick CSL. Because of the ultralow Pt loading and micrometer range thickness of SWNT-based CSLs, we employed a direct measurement of the surface area on the gas diffusion electrode in order to relate the fuel cell performance with the ECSA measurements. In addition, we conducted traditional ECSA measurements on ultra-thin SWNT-Pt thin films deposited on glassy carbon electrodes, and obtained an excellent correlation between the data sets.

Figure 4a presents cyclic voltammetry (CV) ECSA measurements for the Pt loaded SWNTs conducted in 0.5 M H_2SO_4 under nitrogen atmosphere at a scan rate 50 mV/s. The ECSA values were calculated by integrating the charge collected in the hydrogen desorption region after double layer correction under the assumption that a monolayer of hydrogen requires 0.21 mC/cm^2 for its oxidation. As shown in Figure 4b, the lowest ECSA was obtained for the SWNT-HF material which also exhibited a very low BET surface area (Figure 3c). This material shows densely packed thin SWNT-HF bundles (Figure 2d), and the carboxylated fragments occupy the interbundle space blocking access to the Pt nanoparticles. As the COOH acid content decreases, the ECSA increases in correlation with the increased pore size (Figure 2) and decreased presence of carboxylic fragments, but the rate of the ECSA increase is slower than the corresponding increase of the BET surface area (Figure 3c). After reaching a maximum in the case of the SWNT-LF CSL the ECSA decreases by more than 2 times for SWNT-NF in contrast with the corresponding 2.5 fold increase of the BET surface area.

Several factors may contribute to the difference in the dependence of the ECSA and BET surface area on the SWNT carboxylic acid content. First, it should be noted that interstitial (intertube) space within the bundles contributes to the BET surface area but is not accessible to the Pt catalyst nanoparticles. A decrease of acid content leads to an increased bundle size, and thereby increases the interstitial fraction of the BET surface area corresponding to channels that do not contribute to the electro-catalyst activity. Second, with decreasing COOH content we observed an increased aggregation of the Pt catalyst nanoparticles (Figure 2e–h), which would naturally suppress the catalytic activity. The highest ECSA of ~ 60 ± 5 m^2/g was observed for the SWNT-LF material, which combines the advantages of high porosity and BET surface area with the presence of a sufficient concentration of carboxylic groups to anchor the catalyst on the SWNT surface.

For fuel cell testing the SWNT materials were utilized at the cathode electrodes at a loading of 0.03 mg$_{Pt}$/cm^2 in otherwise identical MEA structures, as presented in Figure 5a. For the anode electrode a conventional XC72 carbon black (ETek, Inc.) based CSL was utilized

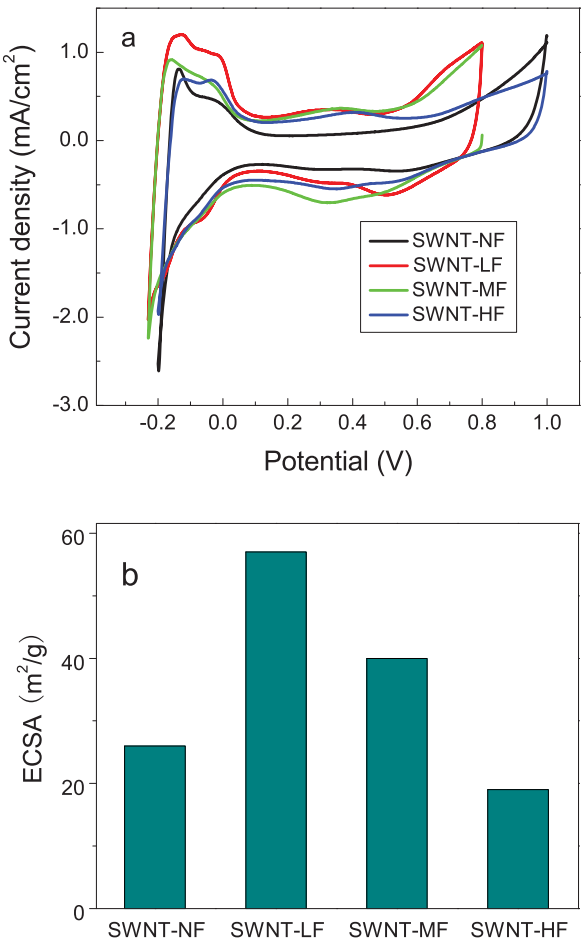

Figure 4 | Electrochemical characterizations. (a) Cyclic voltammograms of Pt loaded SWNTs (b) Electrochemical surface area (ECSA) of Pt supported SWNTs.

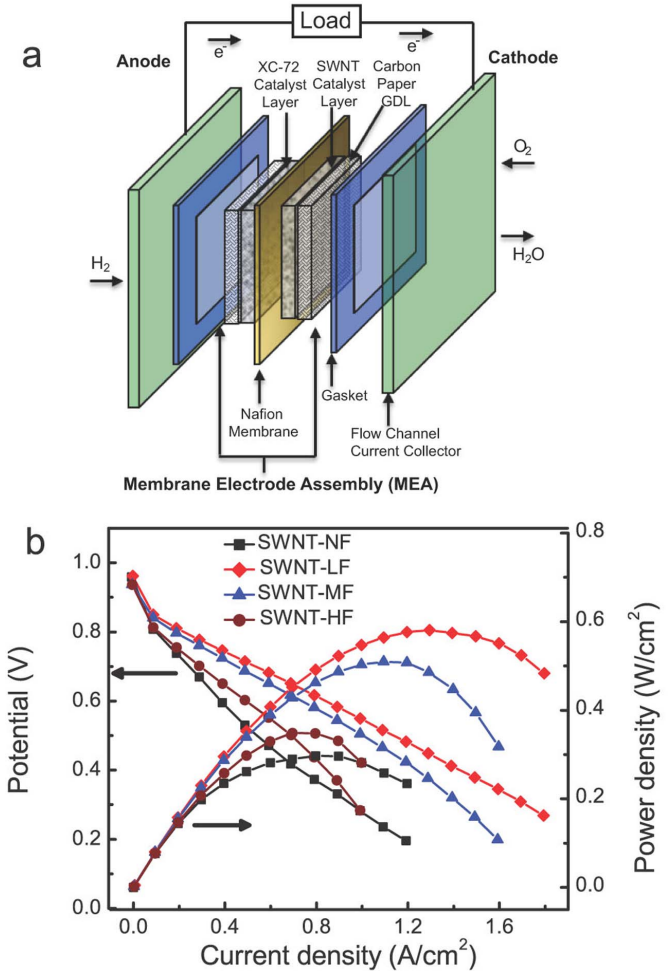

Figure 5 | MEA performance of SWNT catalyst supports. (a) Schematic of MEA with carbon black anode and SWNT cathode catalyst support layer and (b) Fuel cell performance of various SWNT catalyst support layers.

with a loading of 0.2 mg_{Pt}/cm^2. The nafion membrane (DuPont NRE-212) was sandwiched between the anode and cathode (area of 5 cm^2) by hot pressing at 140°C for 3 min at a pressure of 40 kg/cm^2 (Figure S3). Note that the SWNT-CSLs used in this study utilize no nafion in the catalyst layer because the SWNT thin film CSL provides the proton transport. Hydrogen and oxygen were used at the anode and cathode, with a flow rate of 0.2 SLM under a pressure of 35 or 22 psig at an operating temperature of 70 or 80°C.

Figure 5b compares the performance of the MEAs with different cathode CSLs; the lowest MEA performance corresponds to the SWNT-NF and SWNT-HF based cathodes in accord with their low ECSA values. The main cause for the low MEA performance of SWNT-NF cathode material is catalyst aggregation (Figure 2e), while the SWNT-HF based cathode suffers from blocking of the Pt nanoparticles by carboxylic functional groups and suppressed mass transport due to low porosity and high hydrophilicity of the SWNT-HF network. The SWNT-LF and SWNT-MF MEAs show significantly better performance in correlation with the high ECSA values of the corresponding cathodes (Figure 4). The performances of MEAs with SWNT-MF and SWNT-LF cathodes are very similar up to current densities 0.7 A/cm^2; at higher current densities the performance of the MEA with SWNT-MF based cathode degrades while the SWNT-LF based MEA holds its performance up to a current density 1.6 A/cm^2. The high current range of fuel cell operation is usually limited by mass transport[28], which is improved in case of SWNT-LF CSL due to increased porosity and reduced hydrophilicity as a result of the reduction in COOH groups. Thus by adjusting the chemical processing of the catalyst support layer, we were able to optimize the concentration of functional groups, SWNT bundle size, and the SWNT network porosity to achieve improved CSL performance. Because of their high performance the SWNT-LF and SWNT-MF materials were selected for further optimization, as discussed below.

In order to achieve the 2017 DOE technical targets, the Pt loading must be further reduced while maintaining efficient MEA performance. For this purpose the MEA configuration was modified by substituting the 0.2 mg_{Pt}/cm^2 loaded carbon black anode with a SWNT-MF based CSL with a Pt loading of 0.03 mg/cm^2, while on the cathode side the Pt- SWNT-LF was used with the same Pt loading of 0.03 mg/cm^2, resulting in total Pt loading of 0.06 mg/cm^2. Figure 6a shows that the performance of the resulting MEA does not degrade despite the significantly reduced Pt loading at the anode. Moreover, presentation of the results in terms of Pt mass activity in Figure 6b reveals a significant advantage to the utilization of the all-SWNT cathode and anode CSL, demonstrating a fourfold improvement in Pt utilization efficiency.

Discussion

Some of the SWNT-based MEA performance data is benchmarked against the DOE 2017 technical targets in Figure 7. Compared to a conventional all CB MEA with a total Pt loading of 0.8 mg_{Pt}/cm^2 [52], we have reduced the total Pt loading to 0.23 mg_{Pt}/cm^2 with a combination of 0.2 mg_{Pt}/cm^2 carbon black anode CSL and 0.03 mg_{Pt}/cm^2 SWNT cathode CSL. We further reduced the total Pt loading by

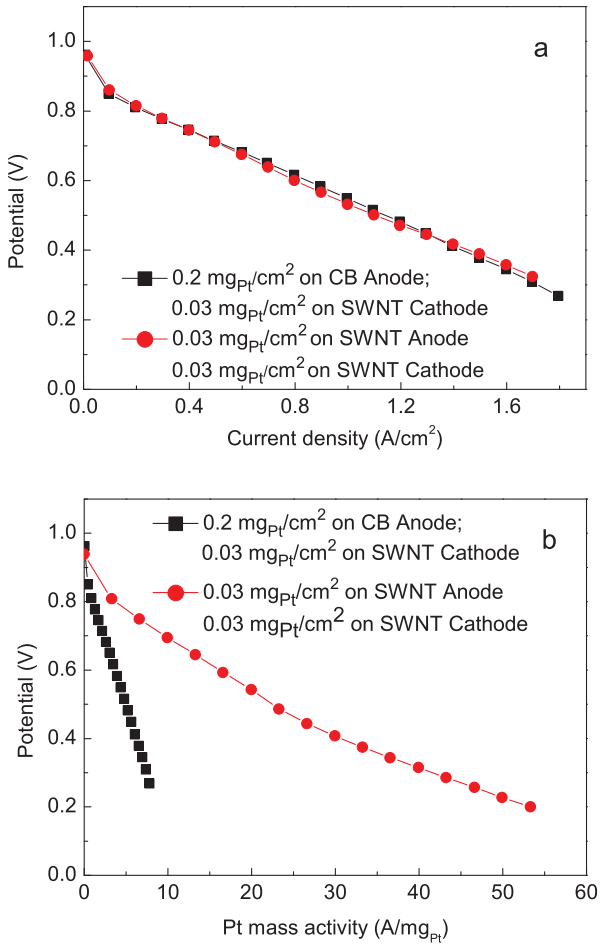

Figure 6 | High mass activity of low Pt-SWNT electrodes. (a) Fuel cell performance of high Pt carbon black (CB) anode (black), compared to low Pt-SWNT anode (red); (b) Mass activity curves for high Pt-CB anode (black), and low Pt-SWNT anode (red).

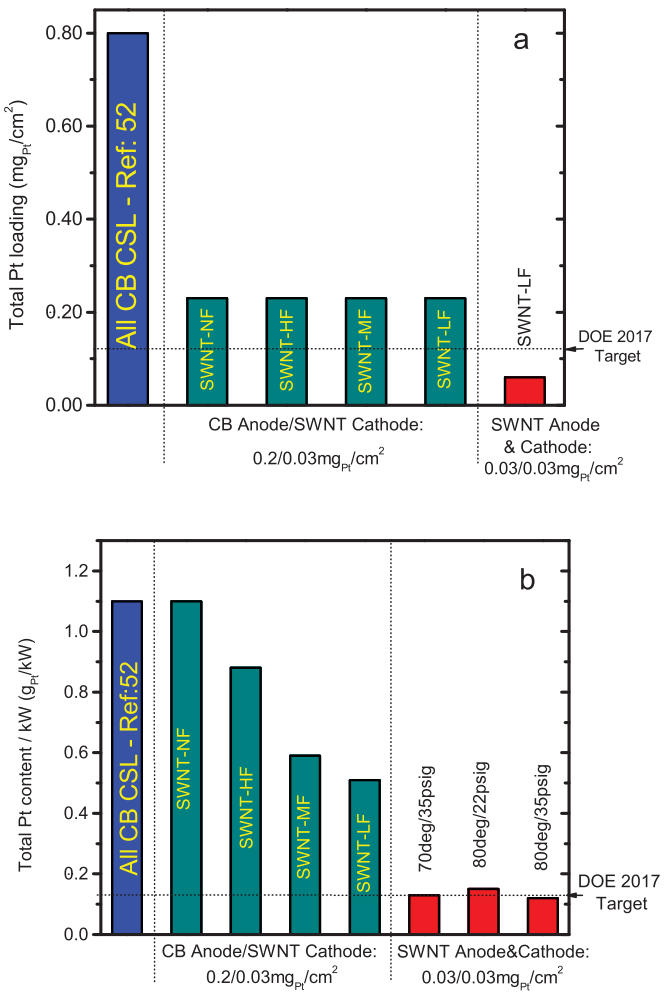

Figure 7 | Benchmark of MEA performance against DOE targets. (a) Total Pt loading per cm^2 (b) Total Pt content per kW.

making both CSLs based on SWNTs with total Pt loading of 0.06 mg_{Pt}/cm^2, well below the DOE 2017 target for Pt group metals of 0.125 mg_{PGM}/cm^2 (Figure 7a). The DOE 2017 technical target for Pt per kW of generated power at V = 0.65 V, requires a figure below 0.125 g_{Pt}/kW. Figure 7b shows an improvement in this parameter as a result of the optimized SWNT acid content on the cathode CSL in the presence of the CB anode with conventional Pt loading of 0.2 mg/cm^2. Utilization of the all-SWNT low Pt loading cathode and anode CSLs attains a level of 0.12 g_{Pt}/kW, thereby satisfying the DOE target, although this value was achieved at pressure of 35 psig at 80°C, while DOE requires an MEA test pressure of 22 psig.

The performance of the SWNT-based PEMFC needs further improvement in order to reach other important DOE targets, for example, the rated power of 1 W/cm^2 at V = 0.65 V for which our MEA shows a value ~ 0.5 W/cm^2. Some of these targets can be achieved by further optimizing the current Pt-SWNT CSL within the Pt loading window 0.06–0.125 mg/cm^2. Reaching the other benchmarks, especially related to the catalyst activation at high fuel cell voltage (V = 0.90 V), would require the combination of the SWNT-based CSL with a novel catalyst system with improved ORR, perhaps relying on approaches under investigation in other laboratories, thereby enabling PEMFC commercialization[2,3,15,19,20,29,36,37].

One of the most important requirements is long term stability of the MEA performance. Here, for initial evaluation, we conducted accelerated stability test of the SWNT-LF CSL at a loading 0.03 mg_{Pt}/cm^2 using cyclic voltammetry to measure the ECSA value as a function of the number of cycles. Figure 8 shows that the surface area of Pt catalyst decreases by less than 5% after 5000 cycles. More extensive long term stability testing needs to be conducted according to DOE requirements, but these initial results show an excellent corrosion stability of the SWNTs and demonstrate the potential of SWNTs as a catalyst support in comparison to current commercial materials, which show a loss of more than 30% of the Pt surface area during similar tests[53–55].

Single-walled carbon nanotubes were chemically processed to achieve the optimal SWNT bundle size and the optimum concentration of carboxylic acid functional groups thereby resulting in efficiently anchored Pt catalyst nanoparticles, and optimum SWNT film porosity, and hydrophilicity. The resulting materials allowed the construction of a prototype SWNT-based PEMFC with total MEA Pt loading reduced to 0.06 mg_{Pt}/cm^2, well below 0.125 mg_{Pt}/cm^2 technical target set by DOE for 2017. This prototype PEMFC also approaches the technical target for the total Pt content per kW of power (<0.125 g_{PGM}/kW) at a cell potential 0.65 V: a value of 0.15 g_{Pt}/kW was achieved at 80°C/22 psig testing conditions, which was further reduced to 0.12 g_{Pt}/kW at 35 psig back pressure. Cyclic voltammetry based accelerated stability tests showed only 5% ECSA reduction after 5000 cycles. The SWNT thin film based CSL involves a wet-ink process that is easily scalable and compatible with the conventional catalyst layer coating technologies thus offering an attractive route to the manufacture of highly efficient, compact automotive fuel cells.

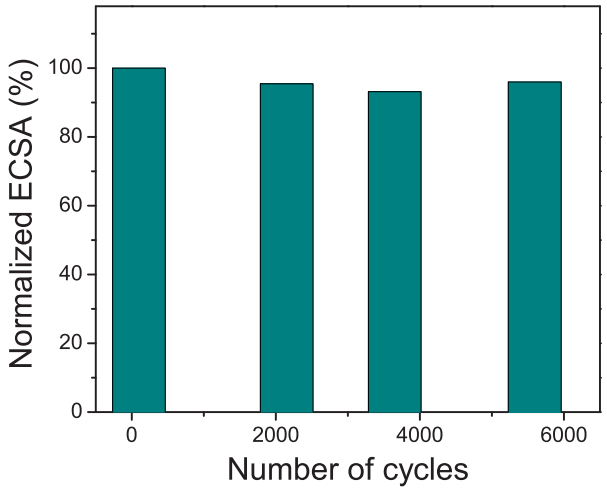

Figure 8 | Accelerated stability test. Electrochemical stability testing of SWNT-LF CSL using cyclic voltammetry.

Methods

As-prepared SWNTs (AP-SWNTs) produced by the arc-discharge method were obtained from Carbon Solutions Inc., Riverside, CA.

The carboxylic acid content in the oxidized SWNTs was determined by directly neutralizing each of the materials with NaOH according literature procedures[48,56]. Briefly, 100 mg of SWNT-COOH material was combined with 25 mL of 0.0125 M NaOH in a sealed polyethylene container and stirred under Ar atmosphere for 48 h. After 48 h the pH was measured with a Corning 445 pH meter and this value was compared to a blank solution (without SWNT material).

The SWNTs were loaded with Pt as follows: 228 mg of SWNT were sonicated overnight in 40 mL of ethylene glycol (EG) and then 263 mg of H_2PtCl_6 added under an Ar atmosphere. The pH of the slurry was adjusted to 11–12 using NaOH and the temperature increased to 135°C and allowed to stir for 3 hrs. After the reaction, the pH of the slurry was decreased to 2 using HCl and washed with excess water three times using a centrifugation/decantation process to remove excess EG. The wet cake of Pt loaded SWNTs was suspended in 250 mL of distilled water to obtain a 1–2 mg/mL dispersion. This dispersion was sonicated 2 hours and further diluted with ethanol to obtain a 0.1 mg/mL dispersion of Pt-SWNTs.

Scanning electron microscopy (SEM) images were obtained from a Philips XL30-FEG instrument operating at 10 kV. TEM images were obtained from Technai 12 operating at 120 kV using an ethanol dispersion of Pt loaded SWNTs. Thermogravimetric analyses of Pt-SWNTs were measured in air at a heating rate of 5°C/min using a Perkin-Elmer Pyris 1 Thermal Analyzer. Cyclic voltammetry experiments were carried out using a three electrode system on a CH Instrument potentiostat (model 1140). The working electrode was fabricated to expose 1 cm^2 active area of the CSL in the GDE by covering other parts with Teflon tape. Pt wire and Ag/AgCl were used as counter and reference electrodes, respectively, and all experiments were carried out under nitrogen atmosphere in 0.5 M H_2SO_4 at a 50 mV/s scan rate. BET surface area was estimated from nitrogen adsorption measured at 77 K using a Quantachrome Autosorb-1 after degassing the samples at 150°C for 2 hrs.

The dispersion of Pt-SWNTs was filtered through a carbon fiber paper GDL coated with a hydrophobic microporous layer (SGL-GDL 25BC) to form a thin film catalyst support layer (CSL) with 0.03 mg_{Pt}/cm^2. A cross sectional image is available in Supplementary Information Figure S3. A SWNT-CSL (0.03 mg_{Pt}/cm^2) without any additional nafion on the SGL-GDL 25BC described above was used as the cathode/anode for all fuel cell tests. The high Pt loaded anode CSLs made of carbon black were prepared by sonicating 20% Pt-XC72 (E-Tek) and nafion (Ion Power Inc.) in water and isopropanol and were sprayed onto a SGL-GDL 25BC until a loading of 0.2 mg Pt/cm^2 was achieved and the nafion content was 35 wt% with respect to the total dry weight of the ink. The Nafion membrane (DuPont NRE-212) was sandwiched between anode and cathode (area of 5 cm^2) by hot pressing at 140°C for 3 min at a pressure of 40 Kg/cm^2 (Supplementary Information Figure S4). Hydrogen and oxygen were used at the anode and cathode, with a flow rate of 0.2 SLM under a pressure of 35 or 22 psig. Anode and cathode humidifier temperatures were held at 80°C and the cell temperature was maintained at 70 or 80°C. Polarization curves were measured on a University Model fuel cell test station (Fuel Cell Technologies, Inc.).

1. Debe, M. *Handbook of Fuel Cells - Fundamental, Technology and Applications* **Vol. 3** (John Wiley and Sons, 2003).
2. Wagner, F. T., Lakshmanan, B. & Mathias, M. F. Electrochemistry and the future of the automobile. *J. Phys. Chem. Lett.* **1**, 2204–2219 (2010).
3. Debe, M. K. Electrocatalyst approaches and challenges for automotive fuel cells. *Nature* **486**, 43–51 (2012).
4. US-DRIVE: Fuel Cell Target Tables, http://www.uscar.org/commands/files_download.php?files_id=279 (07- 27- 2011).
5. The US Department of Energy (DOE). *Energy Efficiency and Renewable Energy* http://www.eere.energy.gov/hydrogenandfuelcells/mypp/pdfs/fuel_cells.pdf and the *US DRIVE Fuel Cell Technical Team Technology Roadmap* (revised 25 January 2012) http://www.uscar.org/guest/teams/17/Fuel-Cell-Tech-Team.
6. Eberle, U., Muller, B. & von Helmolt, R. Fuel cell electric vehicles and hydrogen infrastructure: Status 2012. *Ener. Environ. Sci.* **5**, 8780–8798 (2012).
7. Debe, M. K., Schmoeckel, A. K., Vernstrom, G. D. & Atanasoski, R. High voltage stability of nanostructured thin film catalysts for PEM fuel cells. *J. Power Sources* **161**, 1002–1011 (2006).
8. Stamenkovic, V. R. *et al.* Improved oxygen reduction activity on $Pt_3Ni(111)$ via increased surface site availability. *Science* **315**, 493–497 (2007).
9. Stamenkovic, V. R. *et al.* Trends in electrocatalysis on extended and nanoscale Pt-bimetallic alloy surfaces. *Nat. Mater.* **6**, 241–247 (2007).
10. Lim, B. *et al.* Pd-Pt bimetallic nanodendrites with high activity for oxygen reduction. *Science* **324**, 1302–1305 (2009).

11. Beard, K. D. *et al.* Preparation and structural analysis of carbon-supported Co core/Pt shell electrocatalysts using electroless deposition methods. *ACS Nano* **3**, 2841–2853 (2009).
12. Wu, J. B. *et al.* Truncated octahedral Pt_3Ni oxygen reduction reaction electrocatalysts. *J. Am. Chem. Soc.* **132**, 4984 (2010).
13. Wanjala, B. N. *et al.* Thermal treatment of PtNiCo electrocatalysts: Effects of nanoscale strain and structure on the activity and stability for the oxygen reduction reaction. *J. Phys. Chem. C* **114**, 17580–17590 (2010).
14. Sun, S. *et al.* A highly durable platinum nanocatalyst for proton exchange membrane fuel cells: Multiarmed star like nanowire single crystal. *Angew. Chem. Int. Ed.* **50**, 422–426 (2010).
15. Debe, M. K. *et al.* in U.S. Department of Energy: Hydrogen and Fuel Cell Program, "Advanced cathode catalysts and supports for PEM fuel cells".http://www.hydrogen.energy.gov/pdfs/progress10/v_e_1_debe.pdf (08- 24- 2011).
16. Wang, C., Daimon, H. & Sun, S. H. Dumbbell-like Pt-Fe_3O_4 nanoparticles and their enhanced catalysis for oxygen reduction reaction. *Nano Lett.* **9**, 1493–1496 (2009).
17. Choi, J. Y., Higgins, D. & Chen, Z. W. Highly durable graphene nanosheet supported iron catalyst for oxygen reduction reaction in PEM fuel cells. *J. Electrochem. Soc.* **159**, B87–B90 (2012).
18. Higgins, D. C., Ye, S. Y., Knights, S. & Chen, Z. W. Highly durable platinum-cobalt nanowires by microwave irradiation as oxygen reduction catalyst for PEM fuel cell. *Electrochem. Solid State Lett.* **15**, B83–B85 (2012).
19. Sasaki, K. *et al.* Core-protected platinum monolayer shell high-stability electrocatalysts for fuel-cell cathodes. *Angew. Chem. Int. Ed.* **49**, 8602–8607 (2010).
20. Wang, J. X. *et al.* Oxygen reduction on well-defined core-shell nanocatalysts: Particle size, facet, and Pt shell thickness effects. *J. Am. Chem. Soc.* **131**, 17298–17302 (2009).
21. Wang, D. L. *et al.* Facile synthesis of carbon-supported Pd-Co core-shell nanoparticles as oxygen reduction electrocatalysts and their enhanced activity and stability with monolayer Pt decoration. *Chem. Mater.* **24**, 2274–2281 (2012).
22. Chen, Z. W., Waje, M., Li, W. Z. & Yan, Y. S. Supportless Pt and PtPd nanotubes as electrocatalysts for oxygen-reduction reactions. *Angew. Chem. Int. Ed.* **46**, 4060–4063 (2007).
23. Alia, S. M. *et al.* Porous platinum nanotubes for oxygen reduction and methanol oxidation reactions. *Adv. Func. Mater.* **20**, 3742–3746 (2010).
24. Lefevre, M., Proietti, E., Jaouen, F. & Dodelet, J. P. Iron-based catalysts with improved oxygen reduction activity in polymer electrolyte fuel cells. *Science* **324**, 71–74 (2009).
25. Wang, S. Y., Yu, D. S. & Dai, L. M. Polyelectrolyte functionalized carbon nanotubes as efficient metal-free electrocatalysts for oxygen reduction. *J. Am. Chem. Soc.* **133**, 5182–5185 (2011).
26. Wu, G., More, K. L., Johnston, C. M. & Zelenay, P. High-performance electrocatalysts for oxygen reduction derived from polyaniline, iron, and cobalt. *Science* **332**, 443–447 (2011).
27. Tang, J. *et al.* Carbon nanotube free standing membrane of Pt/SWNTs as catalysts layer in hydrogen fuel cells. *Aus. J. Chem.* **60**, 528–532 (2007).
28. Ramesh, P., Itkis, M. E., Tang, J. M. & Haddon, R. C. SWNT-MWNT hybrid architecture for proton exchange membrane fuel cell cathodes. *J. Phys. Chem. C* **112**, 9089–9094 (2008).
29. Zhu, W. *et al.* Ultra-low platinum loading high-performance PEMFCs using buckypaper-supported electrodes. *Electrochem. Commun.* **12**, 1654–1657 (2010).
30. Girishkumar, G. *et al.* Single-wall carbon nanotube-based proton exchange membrane assembly for hydrogen fuel cells. *Langmuir* **21**, 8487–8494 (2005).
31. Kongkanand, A., Kuwabata, S., Girishkumar, G. & Kamat, P. Single-wall carbon nanotubes supported platinum nanoparticles with improved electrocatalytic activity for oxygen reduction reaction. *Langmuir* **22**, 2392–2396 (2006).
32. Su, F. B. *et al.* Pt nanoparticles supported on nitrogen-doped porous carbon nanospheres as an electrocatalyst for fuel cells. *Chem. Mater.* **22**, 832–839 (2010).
33. Zhou, Y. *et al.* Enhancement of Pt and Pt-alloy fuel cell catalyst activity and durability via nitrogen-modified carbon supports. *Ener. Environ. Sci.* **3**, 1437 (2010).
34. Lin, J. F., Adame, A. & Kannan, A. M. Development of durable platinum nanocatalyst on carbon nanotubes for proton exchange membrane fuel cells. *J. Electrochem. Soc.* **157**, B846–B851 (2010).
35. Rao, C. V., Reddy, A. L. M., Ishikawa, Y. & Ajayan, P. M. Synthesis and electrocatalytic oxygen reduction activity of graphene-supported Pt_3Co and Pt_3Cr alloy nanoparticles. *Carbon* **49**, 931–936 (2011).
36. Tian, Z. Q. *et al.* A highly order-structured membrane electrode assembly with vertically aligned carbon nanotubes for ultra-low Pt loading PEM fuel cells. *Adv. Ener. Mater.* **1**, 1205–1214 (2011).
37. Zhang, W. M. *et al.* Integrated high-efficiency Pt/carbon nanotube arrays for PEM fuel cells. *Adv. Ener. Mater.* **1**, 671–677 (2011).
38. Xie, X. *et al.* Nano-structured textiles as high-performance aqueous cathodes for microbial fuel cells. *Ener. Environ. Sci.* **4**, 1293–1297 (2011).
39. Xie, X. *et al.* Graphene-sponges as high-performance low-cost anodes for microbial fuel cells. *Ener. Environ. Sci.* **5**, 6862–6866 (2012).
40. Tang, J. M. *et al.* Carbon nanotube free-standing membrane as gas diffusion layer in hydrogen fuel cells. *Micro & Nano Letters* **1**, 62–65 (2006).
41. Tang, J. M. *et al.* High performance hydrogen fuel cells with ultralow Pt loading carbon nanotube thin film catalysts. *J. Phys. Chem. C* **111**, 17901–17904 (2007).
42. Itkis, M. E. *et al.* Optimization of the Ni-Y composition in bulk electric arc synthesis of single-walled carbon nanotubes by use of near-infrared spectroscopy. *J. Phys. Chem. B* **108**, 12770–12775 (2004).
43. Haddon, R. C., Sippel, J., Rinzler, A. G. & Papadimitrakopoulos, F. Purification and separation of carbon nanotubes. *MRS Bull.* **29**, 252–259 (2004).
44. Hu, H. *et al.* Influence of the zeta potential on the dispersability and purification of single-walled carbon nanotubes. *J. Phys. Chem. B* **109**, 11520–11524 (2005).
45. Hu, H., Zhao, B., Itkis, M. E. & Haddon, R. C. Nitric acid purification of single-walled carbon nanotubes. *J. Phys. Chem. B* **107**, 13838–13842 (2003).
46. Hu, H. *et al.* Determination of the acidic sites of purified single-walled carbon nanotubes by acid-base titration. *Chem. Phys. Lett.* **345**, 25–28 (2001).
47. Yu, A. *et al.* Application of centrifugation to the large-scale purification of electric arc produced single-walled carbon nanotubes. *J. Am. Chem. Soc.* **128**, 9902–9908 (2006).
48. Worsley, K. A., Kalinina, I., Bekyarova, E. & Haddon, R. C. Functionalization and dissolution of nitric acid treated single-walled carbon nanotubes. *J. Am. Chem. Soc.* **131**, 18153–18158 (2009).
49. Liu, Z. *et al.* Preparation and characterization of platinum-based electrocatalysts on multiwalled carbon nanotubes for proton exchange membrane fuel cells. *Langmuir* **18**, 4054–4060 (2002).
50. Reddy, A. L. M. & Ramaprabhu, S. Pt/SWNT-Pt/C nanocomposite electrocatalysts for proton-exchange membrane fuel cells. *J. Phys. Chem. C.* **111**, 16138–16146 (2007).
51. Kim, H. T., Lee, J. K. & Kim, J. Platinum-sputtered electrode based on blend of carbon nanotubes and carbon black for polymer electrolyte fuel cell. *J. Power Sources* **180**, 191–194 (2008).
52. Gasteiger, H. A., Kocha, S. S., Sompalli, B. & Wagner, F. T. Activity benchmarks and requirements for Pt, Pt-alloy, and non-Pt oxygen reduction catalysts for PEMFCs. *Appl. Catal. B: Environ.* **56**, 9–35 (2005).
53. Shao, Y. Y., Yin, G. P., Gao, Y. Z. & Shi, P. F. Durability study of Pt/C and Pt/CNTs catalysts under simulated PEM fuel cell conditions. *J. Electrochem. Soc.* **153**, A1093–A1097 (2006).
54. Wang, X., Li, W., Chen, Z., Waje, M. & Yan, Y. Durability investigation of carbon nanotube as catalyst support for proton exchange membrane fuel cell. *J. Power Sources* **158**, 154–159 (2006).
55. Santasalo-Aarnio, A. *et al.* Durability of different carbon nanomaterial supports with PtRu catalyst in a direct methanol fuel cell. *Int. J. Hyd. Ener.* **37**, 3415–3424 (2012).
56. Wu, Z. H., Pittman, C. U. & Gardner, S. D. Nitric-acid oxidation of carbon-fibers and the effects of subsequent treatment in refluxing aqueous NaOH. *Carbon* **33**, 597–605 (1995).

Acknowledgments

This work was supported by DOE under Contract # FAR0014507.

Author contributions

N.J. and P.R. performed the CSL and MEA fabrications, electrochemical and fuel cell measurements. N.J., P.R., E.B., X.T. and F.W. performed the characterization of the carbon nanotube materials. R.C.H contributed to the idea of using SWNT thin films in fuel cells. M.E.I. and R.C.H. designed the study. N.J., P.R., E.B., M.E.I. and R.C.H. contributed to the data analysis, interpretation of the results and preparation of the manuscript. M.E.I., P.R. and R.C.H. wrote the manuscript. All authors discussed the results and commented on the manuscript.

Additional information

Supplementary information accompanies this paper at http://www.nature.com/scientificreports

Competing financial interests: The University of California may elect to file a patent on the work reported.

How to cite this article: Jha, N. *et al.* Functionalized Single-Walled Carbon Nanotube-Based Fuel Cell Benchmarked Against US DOE 2017 Technical Targets. *Sci. Rep.* **3**, 2257; DOI:10.1038/srep02257 (2013).

This work is licensed under a Creative Commons Attribution-NonCommercial-NoDerivs 3.0 Unported license. To view a copy of this license, visit http://creativecommons.org/licenses/by-nc-nd/3.0